Journal Name

ARTICLE TYPE

Cite this: DOI: 10.1039/xxxxxxxxxx

Multi-scale microporous silica microcapsules from gas-in water-in oil emulsions

Zenon Toprakcioglu,[a]‡ Tuuli A. Hakala,[a]‡ Aviad Levin,[a] Christian F. W. Becker,[b] Gonçalo J. L. Bernardes[a,c] and Tuomas P. J. Knowles*[a,d]

Received Date
Accepted Date

DOI: 10.1039/xxxxxxxxxx

www.rsc.org/journalname

Controlling the surface area, pore size and pore volume of microcapsules is a key parameter for modulating their activity in applications including catalytic reactions, delivery strategies or even for cell-based culture assays, yet remains challenging to achieve using conventional bulk techniques. Here we describe a microfluidics-based approach for the formation of monodisperse silica-coated micron-scale porous capsules of controllable sizes. Our methods involves the generation of gas-in water-in oil emulsions, and the subsequent rapid precipitation of silica which forms around the encapsulated gas bubbles resulting in hollow silica capsules with tunable pore sizes. We demonstrate that by varying the gas phase pressure, we can control both the diameter of the bubbles formed and the number of internal bubbles enclosed within the silica microcapsule. Moreover, we further demonstrate, using optical and electron microscopy, that these silica capsules remain stable under particle drying. Such a systematic manner of producing silica-coated microbubbles and porous microparticles thus represents an attractive class of biocompatible material for biomedical and pharmaceutical related applications.

1 Introduction

Nature has optimised the formation of organic-inorganic hybrid materials in a controlled manner over millions of years of evolution. This sophisticated hierarchical natural phenomenon has inspired a wide range of studies for mimicking these processes by using strategies derived from the fields of engineering, chemistry and biology. One remarkable example is the formation of silica encasing diatoms, where intricately patterned walls consisting of amorphous silica, have been the inspiration for the formation of multiple modern materials[1–3]. The interest in biomimetic engineering of silica is not only to produce nanostructured materials with unique properties, but also the possibility to obtain a low-cost source of natural material that requires minimal processing[4]. Synthetic bulk approaches of producing mesoporous silica structures by means of using surfactant micelles as templates for silica precipitation, have resulted in restricting the pore size down to 10 nm[5,6], while triblock copolymers with anionic surfactants[7] and butanol[8] have also been employed in the formation of mesoporous silica structures with different pore sizes. Moreover, colloids which have a larger size variety can similarly be used as templates to vary pore diameters[9]. Additionally, bulk-emulsifaction techniques for the production of spherical porous silica particles have been employed[10–12]. However, systematic control over internal pore dimensions on the micrometer scale (∼1-20) is challenging to achieve.

The encapsulation of microbubbles has recently been demonstrated in the context of modulating the porosity of microcapsules for a wide range of biomedical related applications[13,14] such as targeted drug delivery[15,16], catalytic reactions[17], waste water treatment[18] and as tumour/thrombus-destruction materials[19]. Moreover, hollow particles have also attracted attention in the field of energy-storage[20] and in cell culture assays[13,14]. Furthermore, bubbles form the basis of generating foamed porous materials which are essential in the cosmetics, pharmaceutical and food industries[15,21]. Such porous materials may offer orthogonal routes for controlled release of chemicals and are thus quintessential in these industries. There are numerous ways of producing such multi-phase systems[14]. Typically bulk processing techniques or ultrasonic approaches allow for the encapsulation of microbubbles, however, such routes lack in both control over the number of encapsulated bubbles and their relative size[22,23]. To that effect, microfluidic strategies, and in particu-

[a] Department of Chemistry, University of Cambridge, Lensfield Road, Cambridge CB2 1EW, UK
[b] Institute of Biological Chemistry, Faculty of Chemistry, University of Vienna, Wahringer Str.38, 1090, Vienna, Austria
[c] Instituto de Medicina Molecular, Faculdade de Medicina de Universidad de Lisboa, 1649-028 Lisboa, Portugal
[d] Cavendish Laboratory, Department of Physics, J J Thomson Avenue, Cambridge CB3 OHE, UK
* Corresponding Author; Email: tpjk2@cam.ac.uk
‡ These authors contributed equally to this work

lar droplet-based microfluidics, offer significant advantages[24–29]. These strategies give high control over monodispersity and composition, and by forming emulsions drop-by-drop polymeric and protein based particles of various shapes and sizes have been generated.[24,30] In particular, however, the use of silica for the generation of such microporous structures offers advantageous routes due to its biocompatability and ease of production[31].

Here, we demonstrate that by using a non-planar microfluidic device, monodisperse gas-in water-in oil emulsions can be generated in a robust and and precise manner. We further show that the number of internal gas bubbles within the external aqueous droplet can be specifically controlled by varying the pressure at which gas is injected, while keeping the liquid phase flow rates constant. Moreover, by using a silicic acid/buffer system as the aqueous phase, the precipitation of silica occurred almost instantaneously around the encapsulated gas bubbles, allowing for the formation of hollow silica capsules with controllable pore sizes on the micrometer scale. Furthermore, electron microscopy was conducted in order to investigate the morphology of the silica beads. Finally, SEM micrographs revealed that the microcapsules remain stable when dried and cross-sectional images indicate that the internal structure of the particles is full of cavities which correspond to the number and size of previously encapsulated gas bubbles.

2 Experimental Methods

2.1 Device fabrication.

A two-step photolithographic process was utilised to fabricate the master used for casting PDMS devices as has been previously reported[30]. A 25 μm thick negative photo-resist (SU-8 3025, MicroChem) was spin-coated onto a silicon wafer. This in turn, was soft-baked for 15 minutes at 95 °C. The photomask in figure 1b was then placed onto the wafer, exposed under UV light in order to induce polymerisation and then post-baked at 95 °C for 3 minutes. A second 25 μm thick layer (SU-8 3025, MicroChem) was then spin-coated onto the wafer and sof-baked for 30 minutes at 95 °C. The second mask (shown in figure 1a) was aligned with respect to the patterns formed from the first mask. This was in turn exposed to UV light and post-baked for 5 minutes at 95 °C. Finally, to remove uncross-linked photo-resist, the master was developed in Propylene glycol methyl ether acetate (PGMEA, Sigma-Aldrich)

A 10:1 ratio of elastomer PDMS to curing agent (Sylgard 184, DowCorning, Midland, MI) was used to fabricate microfluidic devices. The mixture was cured for 3 hours at 65 °C. The hardened PDMS was cut and peeled off the master, while holes of 0.75 mm were punched on the PDMS. This was then bonded onto a glass slide by treating with a plasma bonder (Diener Electronic, Ebhausen, Germany).

2.2 Droplet formation.

The flow rates within the channels were controlled using neMESYS syringe pumps (Cetoni, Korbussen, Germany). For droplet formation two aqueous phases were used. One of the phases consisted of silicic acid, while the other was comprised of 50 mM sodium phosphate buffer with 2% Tween 20. Furthermore fluorinated oil (Fluorinert FC-40, Sigma Aldrich) containing 2% w/w fluorosurfactant (RAN biotechnologies) was used as the continuous phase. Nitrogen and carbon monoxide gases were used as the inner phase. The formation of droplets was monitored on-chip using a Mikrotron High Speed Camera.

2.3 Scanning Electron microscopy.

The silica-coated microbubbles samples were mounted onto a glass slide and left to dry for 24 hours. This was then placed onto a multi-pin specimen mount. A 5 nm platinum layer was subsequently sputter coated onto the sample and images were obtained using a TESCAN MIRA3 FEG-SEM operating at 5 kV.

3 Results and Discussion

In order to generate microcapsules with variable multi-scale pore sizes, we first generated gas-in water-in oil emulsions (g/w/o). This was done using a non-planar microfluidic device, where the inner phase contained the gas, while the middle and outer phases consisted of silicic acid (with buffer) and oil respectively. Once the silicic acid comes into contact with the sodium phosphate buffer (figure 1), the precipitation of silica occurred rapidly[1] around the encapsulated gas bubbles resulting in the formation of microporous silica capsules. It was determined that by varying the pressure at which gas was injected through the device, while keeping the flow rates of the liquid phases constant, both bubble size but also the number of internal bubbles could be specifically controlled. The bubbles suspended in the aqueous phase, were then encapsulated by the oil phase resulting in the formation of an bubble loaded aqueous droplet in oil. This gas-water-oil (g/w/o) three-phase system was the basis for all subsequent experiments. The silica microparticles were then de-emuslified and re-injected into an aqueous medium, before being imaged using optical and electron microscopy. The latter of which revealed the cavities within the porous microparticles.

3.1 Device design

The silica-coated microcapsules were synthesised using a g/w/o emulsion strategy that relies on the formation of monodisperse micro-droplets.

These consisted of a gas core, surrounded by an aqueous phase, comprised of silicic acid with sodium phosphate buffer, all of which is encapsulated within a continuous immiscible oil phase. In order to generate such droplets, the use of a non-planar microfluidic device design was employed. This ensured that the aqueous phase did not wet the microfluidic channel surface and allowed for successful droplet generation. The master used for all experiments was fabricated using a two-step soft lithography process. To this effect; 25 μm high structures were formed using a film mask (figure 1b) and then aligned with channels fabricated using a second film mask shown in figure 1a. This resulted in the generation of a non-planar device which is schematically depicted in figure 1c (see Methods for additional details on device fabrication).

Typically, droplet generation involves an aqueous phase intersecting with an immiscible oil phase resulting in the formation of

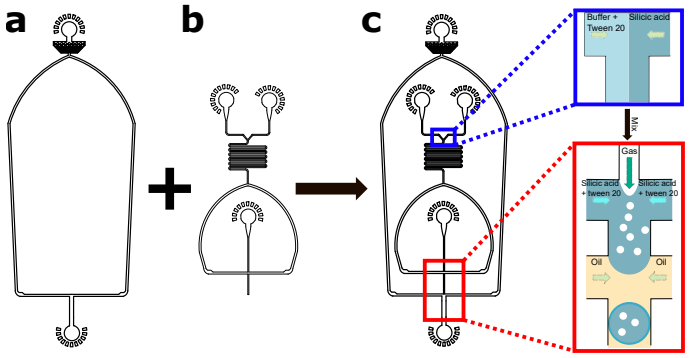

Fig. 1 (a-c) Design of the microfluidic device used. A two-step lithographic process was used in order to fabricate the device shown in **(c)**. **(a)** Mask 1: Outer oil phase inlet with its respective channels and outlet. **(b)** Mask 2: middle and inner phase inlets. The aqueous phase consists of two inlets. Inlet 1: silicic acid. Inlet 2: sodium phosphate buffer with Tween 20. Once these two solutions, intersect, a long channel allows for successful mixing before they reach the gas channel. **(c)** Schematic representation of the device used to generate gas-in water-in oil droplets. The third junction is the non-planar (3-D) junction.

water-in-oil or oil-in-water droplets. However, in order to generate g/w/o emulsions, an additional inlet was introduced. The device architecture consists of two main regions, each of which plays a fundamental role in the operation of the device. In the first region, silicic acid is mixed with sodium phosphate buffer and with Tween 20, as shown in the top right inlet of figure 1c. A long serpentine channel separating this junction from the second junction allows for the two solutions to mix well before being introduced to the channel containing the gas phase. The channel length separating the first and second junction is crucial in increasing the viscosity of the aqueous phase (as the reduction of silicic acid to silica commences upon mixing with the buffer) which in turn allows for successful bubble formation and encapsulation due to increased solution surface tension. The two aqueous solutions could not be pre-mixed before being pumped through the microfluidic channels due to the speed at which the silicic acid and sodium phosphate/Tween 20 solutions precipitate and gel (see figure S1a), which is why they were mixed on-chip. In the second junction, the gas intersects with the silicic acid/sodium phosphate/Tween 20 solution resulting in the production of bubbles. This in turn is encapsulated by the oil phase in the third junction. This entire process of g/w/o monodisperse droplet formation is schematically represented in figure 1c (bottom right inlet).

3.2 Silica-coated microcapsule formation and characterisation

Next, we explored the generation of micron-sized g/w/o emulsions using nitrogen as a model gas. The relationship between the gas pressure and the number of internal bubbles encapsulated was further investigated. This was determined by keeping the respective aqueous phase flow rates (Q_{aq}) constant at 300 μL/h and the outer oil phase flow rate (Q_{oil}) at 800 μL/h, while the gas pressure values ranged from 110 up to 200 mbar. Once formed, the number of encapsulated internal bubbles was determined by high speed imaging and frame by frame analysis of the data. The number of internal bubbles (N) was found by averaging over a total of 10 subsequent droplets. Figure 2a shows g/w/o emulsions which are formed at the third junction of the device.

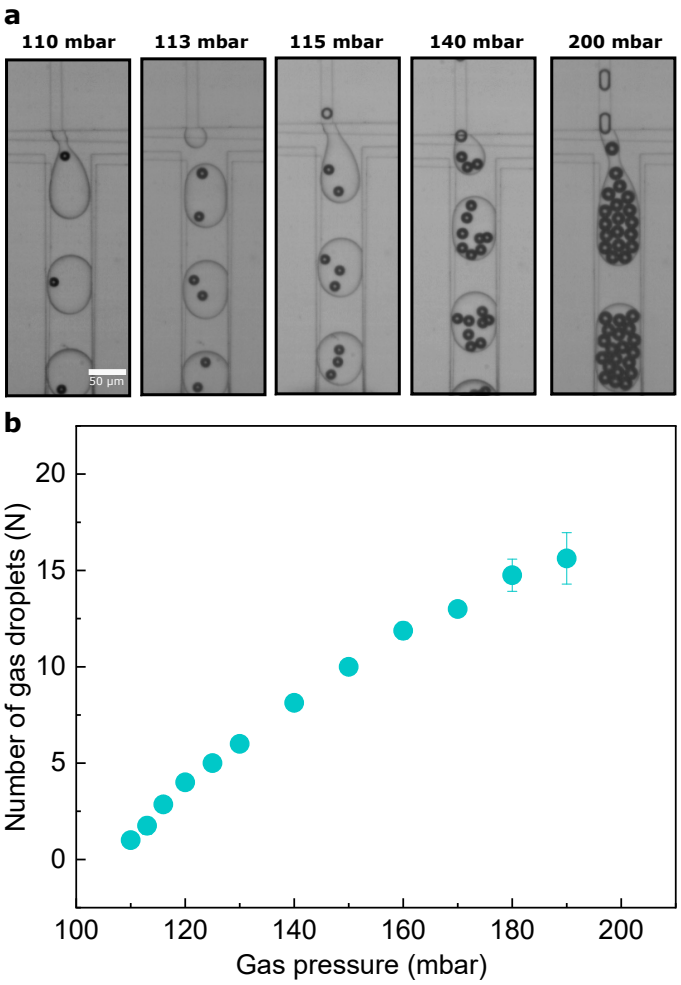

Fig. 2 (a) g/w/o emulsion droplets generated from the microfluidic device for a range of gas pressures when Q_{aq} = 300 μL/h for both phases while Q_{oil} = 800 μL/h. As can be seen from the optical micrographs, the number of internal bubble droplets could be specifically controlled based on the gas pressure, and ranged from N = 1 to N = 20. The scale bar for all images is 50 μm. **(b)** Dependence of the number of internal gas droplets (N) on the pressure exerted within the microchannel.

Figure 2a shows g/w/o emulsions with a range of number of internal bubbles, varying from N = 1 up to N = 20. The precise and systematic control of this microfluidic setup is demonstrated in each of the optical micrographs, with 1, 2, 3, 8 and 20 internal gas bubbles being encapsulated with increasing pressure. Moreover, an optical image showing N = 6 internal bubbles is shown in figure S1b. As expected, the higher the gas pressure, the more internal bubbles that can be encapsulated. Interestingly, a plot of N against gas pressure, which is shown in figure 2b, indicates an almost linear relation, with a gradient close to 0.2. Following formation, droplets were then collected and placed on a cover slide in order to investigate whether the microcapsules remained stable over time. As can be seen in figure 3a-d, not only are the particles stable but during silica precipitation, the gas re-

mains trapped within the droplet long enough for a silica shell to be formed around the bubbles. This allows for a precise way of modulating porosity, which suggests that these microcapsules can be used for various biomedical applications where pore sizes are instrumental. Additionally, the high level of monodisperse droplets and encapsulated bubbles formed using this setup can be seen in the micrographs of figure 3a-d.

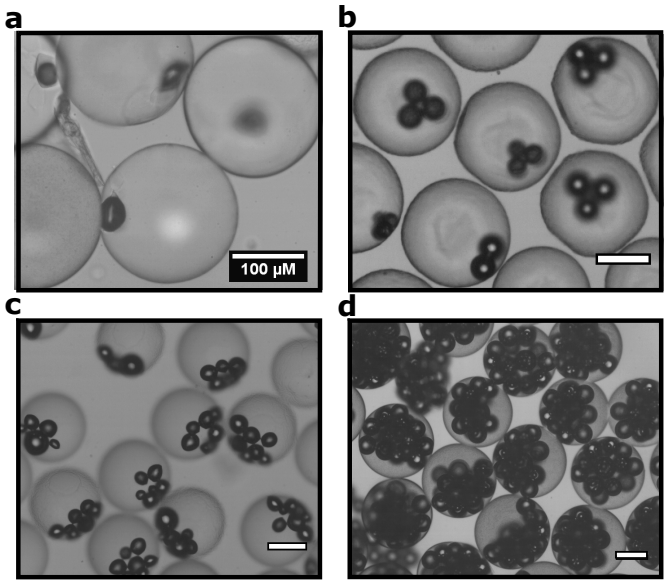

Fig. 3 (a-d) Optical micrographs of g/w/o emulsions with varying numbers of internal gas bubbles placed on a cover slip. It is clear that following their generation, the gas loaded droplets remain stable while drying resulting in the formation of a silica shell around the bubbles. The scale bar for all images is 100 μm.

Scanning electron microscopy (SEM) was conducted on the silica-coated microcapsules in order to further characterise them. Following emulsion generation, droplets were incubated at room temperature for 1 hour before washing and de-emuslification. The silica particles were then re-emulsified in deionised water, placed on a glass slide and left to dry for 24 hours. The SEM images in figure 4a show monodisperse, spherical particles with a rough surface morphology. Moreover, the microcapsules remain mostly stable and do not seem to collapse upon drying. They do, however, shrink by approximately a factor of 2, which is due to the water diffusing out of the microbeads.

The pores that can be seen on the surface of some silica particles is probably the result of a gas bubble coming too close to the droplet interface during silica formation. However, this can be resolved by increasing the viscosity within the aqueous solution during microfluidic droplet generation in order to restrict gas movement within the emulsion. This can either be done by increasing the silicic acid concentration, or by increasing the serpentine length between the first and second junction. Furthermore, cross-sectional micrographs of the particles were taken by cutting the silica beads in half. The images in figure 4b-g reveal the cavities within the capsules where the bubbles were and give an insight into the internal structure of the particle. It is clear that by regulating the number of encapsulated bubbles one can tailor the porosity of microcapsules to the point where molecular release/uptake through the silica network and into the environment can be specifically controlled.

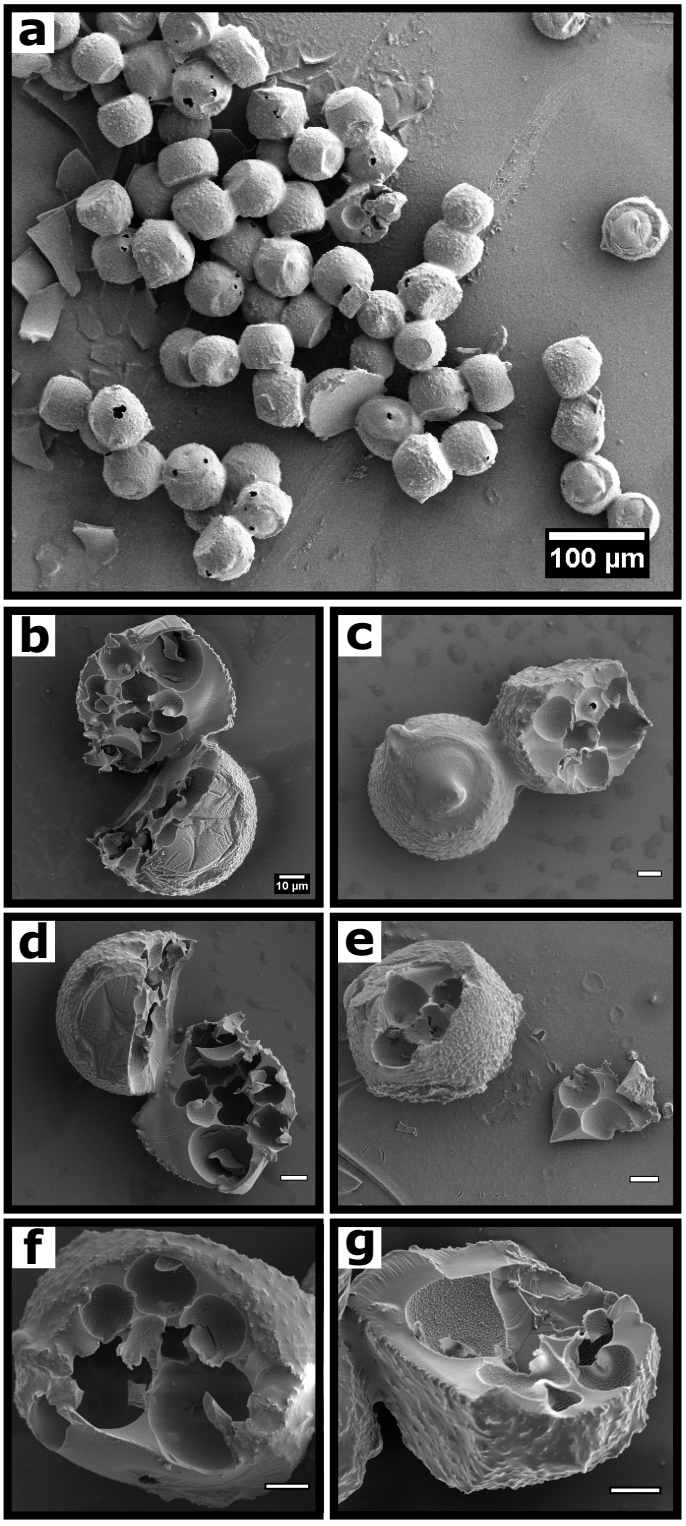

Fig. 4 (a-g) Scanning electron micrographs of silica-coated microcapsules. The microparticles remain stable and do not collapse upon drying. **(b-g)** Cross-sectional micrographs reveal the areas (cavities) within the capsules where the bubbles were. The scale bars depict 10 μm.

4 Conclusions

Controllable generation of monodisperse micro-sized gas-in water-in oil (g/w/o) droplets in a reproducible manner is desirable for next-generation delivery strategies, yet remains challenging. Here, we show that by utilising non-planar microfluidics, a scalable platform for generating silica-coated microcapsules can be developed, mimicking the formation of diatoms in nature. G/w/o droplets were generated on chip, and by mixing silicic acid with sodium phosphate buffer, multiple microbubbles stabilised by a silica shell within the same microcompartment could be formed. We demonstrate that using this approach, control over bubble size and number of encapsulated bubbles within individual capsules can be precisely achieved by varying the pressure at which the gas-phase is introduced on-chip. In addition, following droplet generation, optical microscopy reveals that these emulsions are stable and that the gas remains trapped within the microparticles long enough for the precipitation of silica to form around the bubbles. Moreover, scanning electron micrographs further corroborates that these particles are stable when dried and that cavities formed due to the presence of gas bubbles during droplet generation contribute towards the silica capsule microporous morphology. Such silica-based microcapsules represent a class of biocompatible and non-toxic material, and in conjunction with the high level of control over their formation, these multi-scale microporous capsules have favourable characteristics enabling them to serve as a platform to explore various delivery and related biomedical applications.

Conflicts of interest

There are no conflicts to declare.

Acknowledgements

The research leading to these results has received funding from the European Research Council under the European Union's Seventh Framework Programme (FP7/2007-2013) through the ERC grant PhysProt (agreement n° 337969). We are also grateful for financial support from the EU Horizon 2020 programme (Marie Skłodolwska-Curie ITN G.A. No. 675007 to T.A.H., G.J.L.B. and T.J.P.K.), the Oppenheimer Early Career Fellowship (A.L.), the BBSRC (T.P.J.K.), the Newman Foundation (T.P.J.K.) and the Cambridge Centre for Misfolding Diseases.

Notes and references

1 N. Kröger, S. Lorenz, E. Brunner and M. Sumper, *Science*, 2002, **18**, 584–586.

2 M. Sumper, *Science*, 2002, **295**, 2430–2433.

3 C. C. Lechner and C. F. Becker, *Marine Drugs*, 2015, **13**, 5297–5333.

4 X. W. Sun, Y. X. Zhang and D. Losic, *Journal of Materials Chemistry A*, 2017, **5**, 8847–8859.

5 C. T. Kresge, M. E. Leonowicz, W. J. Roth, J. C. Vartuli and J. S. Beck, *Nature*, 1992, **359**, 710–712.

6 J. S. Beck, J. C. Vartuli, W. J. Roth, M. E. Leonowicz, C. T. Kresge, K. D. Schmitt, C. T. Chu, D. H. Olson, E. W. Sheppard, S. B. McCullen, J. B. Higgins and J. L. Schlenker, *Journal of the American Chemical Society*, 1992, **114**, 10834–10843.

7 D. Chen, Z. Li, Y. Wan, X. Tu, Y. Shi, Z. Chen, W. Shen, C. Yu, B. Tu and D. Zhao, *Journal of Materials Chemistry*, 2006, **16**, 1511–1519.

8 F. Kleitz, S. H. Choi and R. Ryoo, *Chemical Communications*, 2003, **17**, 2136–2137.

9 O. D. Velev, T. A. Jede, R. F. Lobo and A. M. Lenhoff, *Nature*, 1997, **389**, 447–448.

10 N. Andersson, B. Kronberg, R. Corkery and P. Alberius, *Langmuir*, 2007, **23**, 1459–1464.

11 M. M. Dragosavac, G. T. Vladisavljević, R. G. Holdich and M. T. Stillwell, *Langmuir*, 2012, **28**, 134–143.

12 N. Bchellaoui, Z. Hayat, M. Mami, R. Dorbez-Sridi and A. I. El Abed, *Scientific Reports*, 2017, **7**, 16326.

13 R. Chen, P.-F. Dong, J.-H. Xu, Y.-D. Wang and G.-S. Luo, *Lab on a Chip*, 2012, **12**, 3858–3860.

14 J. Wan, A. Bick, M. Sullivan and H. A. Stone, *Advanced Materials*, 2008, **20**, 3314–3318.

15 J. R. Lindner, *Nature Reviews Drug Discovery*, 2004, **3**, 527–532.

16 S. Ramachandran, S. Shaheedha, G. Thirumurugan and M. Dhanaraju, *Current Drug Delivery*, 2010, **7**, 93–97.

17 H. G. Yang and H. C. Zeng, *Journal of Physical Chemistry B*, 2004, **108**, 3492–3495.

18 B. Albijanic, O. Ozdemir, A. V. Nguyen and D. Bradshaw, *Advances in Colloid and Interface Science*, 2010, **159**, 1–21.

19 E. C. Unger, T. Porter, W. Culp, R. Labell, T. Matsunaga and R. Zutshi, *Advanced Drug Delivery Reviews*, 2004, **56**, 1291–1314.

20 C. Wu, Y. Xie, L. Lei, S. Hu and C. OuYang, *Advanced Materials*, 2006, **18**, 1727–1732.

21 R. N. Zúñiga and J. M. Aguilera, *Trends in Food Science and Technology*, 2008, **19**, 176–187.

22 M. V. Artemyev, U. Woggon and R. Wannemacher, *Applied Physics Letters*, 2001, **78**, 1032.

23 J. Bibette, F. Leal-Calderon, V. Schmitt and P. Poulin, *Emulsion Science*, 2007.

24 X. Liu, Z. Toprakcioglu, A. J. Dear, A. Levin, F. S. Ruggeri, C. G. Taylor, M. Hu, J. R. Kumita, M. Andreasen, C. M. Dobson, U. Shimanovich and T. P. J. Knowles, *Macromolecular Rapid Communications*, 2019, **40**, 1800898.

25 P. Garstecki, M. J. Fuerstman, H. a. Stone and G. M. Whitesides, *Lab on a chip*, 2006, **6**, 437–446.

26 A. Rotem, A. R. Abate, A. S. Utada, V. Van Steijn and D. a. Weitz, *Lab on a Chip*, 2012, **12**, 4263.

27 Z. Toprakcioglu, P. K. Challa, A. Levin and T. P. J. Knowles, *Lab on a Chip*, 2018, **18**, 3303–3309.

28 T. Nisisako, S. Okushima and T. Torii, *Soft Matter*, 2005, **1**, 23.

29 R. T. Davies, D. Kim and J. Park, *Journal of Micromechanics and Microengineering*, 2012, **22**, 055003.

30 Z. Toprakcioglu, A. Levin and T. P. J. Knowles, *Biomacromolecules*, 2017, **18**, 3642–3651.

31 F. Tang, L. Li and D. Chen, *Advanced Materials*, 2012, **24**, 1504–1534.